IEEE Access
Multidisciplinary ⋮ Rapid Review ⋮ Open Access Journal

Received 16 November 2022, accepted 3 January 2023, date of publication 23 January 2023, date of current version 27 January 2023.

Digital Object Identifier 10.1109/ACCESS.2023.3239397

RESEARCH ARTICLE

Reduction of Surface Reflection on Dielectric Lens Antenna by Matching Periodic Square-Pillars in 300-GHz Band

BAZILAH BAHAROM[1], (Student Member, IEEE), RYOTA ISHIHARA[1], YOSHIKI SUGIMOTO[1], (Member, IEEE), KUNIO SAKAKIBARA[1], (Senior Member, IEEE), NOBUYOSHI KIKUMA[1], (Senior Member, IEEE), TAKAYUKI ARAI[2], TAKAYOSHI SUGANUMA[2], AND TOMOHIRO SAITO[2]

[1]Department of Electrical and Mechanical Engineering, Nagoya Institute of Technology, Nagoya, Aichi 464-8555, Japan
[2]Enplas Corporation, Kawaguchi, Saitama 332-0034, Japan

Corresponding author: Yoshiki Sugimoto (sugimoto.yoshiki@nitech.ac.jp)

This work was supported by the Ministry of Internal Affairs and Communications of Japan with a Scheme of Research and Development for Expansion of Radio Wave Resources under Grant JPJ000254.

ABSTRACT This study proposes a dielectric lens antenna that implements an impedance matching layer comprising square-pillar periodic structures on the lens surface to reduce the surface reflection formed in the lens from a high-permittivity dielectric material. To ease the fabrication process, the matching structures (MS) implemented on the lens surface are made of the same dielectric material as the dielectric lens through microfabrication structure. The dimensions of the square-pillar periodic MS unit cell are optimized for its period, space occupancy ratio, and height using periodic boundary simulation, considering the plane wave incident. Electromagnetic simulations and experiments to evaluate the effectiveness of the optimized square-pillar periodic MS were conducted. Implementing the square-pillar periodic MS to a lens composed of modified-polyphenylene ether (modified-PPE) with a relative permittivity of 5.34 assists in reducing the surface reflection inside the lens compared with the lens without anti-reflection and improves the peak gain by approximately 2 dB from 250 to 290 GHz.

INDEX TERMS Dielectric lens antenna, surface reflection, periodic structure, terahertz.

I. INTRODUCTION

As millimeter-wave and terahertz-wave frequency bands accommodate a wide frequency bandwidth, wireless communications using frequency bands are expected to provide advanced applications supported by high-speed communications. Because the wave propagation attenuation coefficient in the atmosphere is relatively low, (approximately 300 GHz), research and development using this frequency band are underway [1]. The 252–296 GHz band focuses on high-speed communication systems, such as high-definition video transmission and beyond-5G/6G mobile communication systems [2], [3], [4], [5]. The free space path loss in the 300-GHz band is colossal compared to the frequency bands used for the 4th- and 5th-generation mobile communication systems. In the 300-GHz band, antennas with high directivity and low feeding loss are required to establish a wireless communication link [6], [7].

A dielectric lens antenna is a promising candidate for wide use of communication systems and sensing systems from millimeter-wave band toward terahertz-wave band. In the requirements for future applications of small volumes, the major constraint is related to the antenna's overall size. The objective is to reduce the diameter and total height occupied by the antenna while maintaining the best performance in terms of gain, bandwidth, ease of fabrication, and integration. In addition, a lens antenna is characterized by lower feeding loss and less frequency dependence of the radiation

The associate editor coordinating the review of this manuscript and approving it for publication was Pavlos I. Lazaridis.

characteristics than those in substrate-printed planar antennas because the lens antenna feeds the lens from the primary radiator in a ray principle through-free space.

However, the overall height of the lens antenna limits the mounting space in the housing of the communication systems. Furthermore, if the lens is thick, manufacturing difficulty increases. Thus, conventional methods make lens antennae bulky [8], [9], [10], [11] because of the need for several thicknesses and layers to realize the desired features and performances of their applications.

The focal length of the lens can be reduced by increasing the curvature of the lens surface. Thus, the vacant space secured between the lens and the primary radiator is reduced. Although the lens is thicker with a shorter focal length, this problem can be resolved using a high-permittivity material for the lens, which provides a thin lens curve. However, when the relative permittivity of the lens is much larger than the permittivity of free space, a spatial impedance mismatch occurs in the lens surface reflection. Impedance mismatch must be avoided considerably because the reflection directly causes gain deterioration of the lens antenna.

Recently, various methods to design a lens antenna with a low profile and high gain for the millimeter-wave and terahertz-wave band have been reported. In [12], the concept of a low-profile lens was successfully investigated by replacing a large-aperture single lens with a small lens array. However, the former antenna caused the feeding design and lens shaping to become complex. Next, in [13], a low-profile and high gain in the sub-millimeter-wave lens were achieved; however, a large number of multi-layer leaky wave feeds were required to increase the beam-shaping flexibility.

Therefore, the implementation of a matching layer (ML) to the lens antenna has been extensively studied to overcome the problem of a thicker lens owing to its short focal length and to achieve a low-profile compact antenna in a higher frequency band. In particular, for a lens using a high- permittivity material, the effects of impedance mismatch and lens surface reflections can be alleviated by adding an ML to the lens surface. By contrast, lens thickness can be significantly decreased. It also helps to improve the lens antenna gain to its highest value. In [14], the ML of a discrete dielectric slab with square holes to improve reflection coefficient and gain was proposed. Similar to [15] and [16], anti-reflection surfaces that utilize such microstructures have been actively studied in the fields of optics with the development of microfabrication technology and are called sub-wavelength structures. However, in higher millimeter-wave bands, it is quite difficult to coat or paste the dielectric by different materials with constant thickness and without gap. Most of the ML designs were reported at lower millimeter-wave frequencies. This is because of the awareness of the difficulty of developing and fabrication constraints at this terahertz frequency. Bonding ML without air gaps between different dielectrics is extremely difficult in the 300-GHz frequency band. Lens antennas with matching layer on the surface has been developed in the 300-GHz band by the same group with [14].

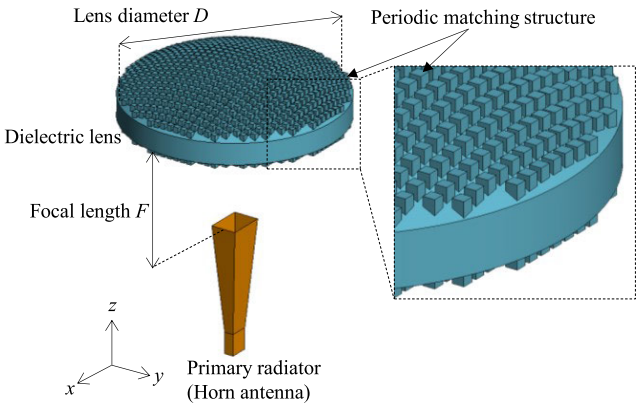

FIGURE 1. Dielectric lens antenna with a square-pillar periodic MS.

However, detail design techniques and effect have not been discussed.

Therefore, this study used modified-Polyphenylene ether (modified-PPE), which has a higher permittivity than that of polypropylene, is commonly used as a dielectric material and has better manufacturability [17], [18]. Low-profile lens antenna with short focal length and thin lens was developed in this work. Furthermore, we also implemented a dielectric lens antenna with an effective impedance matching structure (MS) function on the lens surfaces using a micro-fabricated periodic structure. The anti-reflection structure comprised single dielectric material in the sub-terahertz band. Optimization of the periodic structure for inclined incidence of TE and TM waves for lens surface operation and detail measured evaluation of the effect of the matching structure have done in low-profile design. The small physical antenna size with a total height from the aperture of the primary radiator of 13.7 mm and a lens diameter of 10 mm with maintaining high performance and a relatively easy design and manufacturing process is developed in this work. The remainder of this paper is organized as follows. Section II introduces the design method for a dielectric lens antenna with a square-pillar periodic MS. The optimization of the MS using a periodic structure simulation is described in Section III. In addition, the effectiveness of the proposed antenna is demonstrated by comparing the radiation characteristics of lens antennas with and without the optimized MS. The simulation validity is presented in Section IV. Finally, conclusions are presented in Section V.

II. GEOMETRY AND THEORY

A. DIELECTRIC LENS ANTENNA WITH A MATCHING STRUCTURE

This section describes the proposed dielectric lens antenna with an MS. We focus on a simple dielectric lens antenna comprising a dielectric lens and a horn antenna primary radiator, as shown in Fig. 1. The horn antenna is made of metal and is fed from a WR-3 standard waveguide. The horn adjusts its aperture size by considering the primary illumination pattern

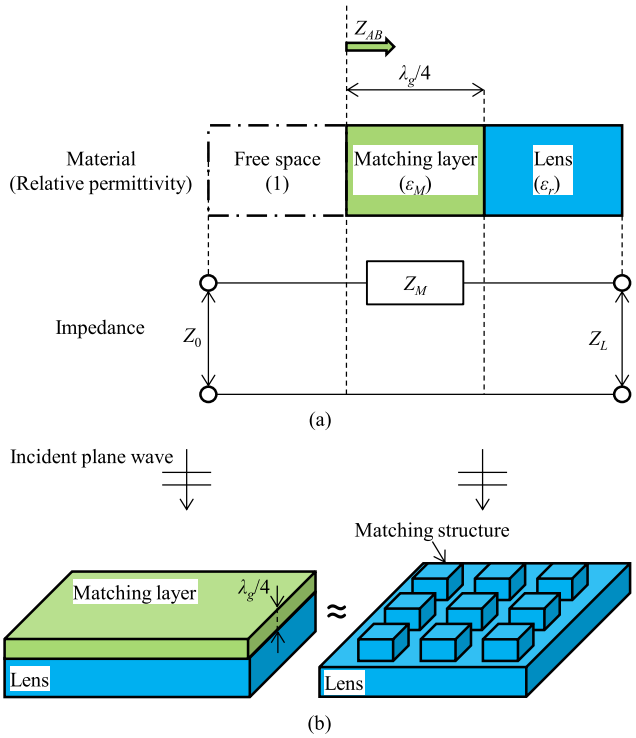

FIGURE 2. Reflection reduction on the lens surface by impedance transformation. (a) Equivalent circuit expression. (b) Geometric approximation of the surface ML by square-pillar periodic with a single relative permittivity material.

of the dielectric lens. The appropriate primary radiation level at the lens edge with respect to the center of the lens bottom (edge level) is approximately −10 dB owing to the trade-off between the spillover loss and lens aperture efficiency. The aperture size of the horn antenna designed to the edge level in this is −10 dB [19].

As for the dielectric lens, an axisymmetric curve plano-convex lens with a flat surface on the side of the primary radiator and a curved surface in the main radiation direction is used [20]. Plano-convex lens has feature such as simple design shape and easier comparison in 300 GHz band. It has the advantage of being easy to process matching square-pillars, which will described in Section II-B, because bottom side of the lens is completely flat. To derive the curved surface coordinates of the plano-convex lens, the electromagnetic wave radiated from the primary radiator is approximated by an optical ray. Thus, the coordinates of the curves are derived by solving simultaneous equations comprising Snell's law and the law of constant optical path length from the primary radiator to the lens aperture surface [21], [22]. The lens diameter defined as D, and the focal length of the lens is defined as F, which are the parameters required to calculate the lens curve. The lens diameter D was determined from the required peak gain. The focal length F can be determined arbitrarily by calculating the lens curve. The phase center of the horn antenna should be optimally placed at the focal position of the lens, however in this study, the focal position of the lens was placed at the center of the horn aperture to simplify the design. When the horn length is ignored, the antenna height of a plano-convex lens antenna is determined by the summation of the focal length and thickness of the lens. The lens diameter D was fixed from the required gain. The height of the entire lens antenna can be reduced by setting a short focal length when deriving the coordinates of the lens curve. Therefore, it is effective to design the ratio of the focal length to the lens diameter F/D as small for designing a low-profile lens antenna. However, with a smaller F/D, the difference in distances from the focal point to the center and to the edge is larger. Therefore, the thickness of the lens was increased to make the lengths of the two optical paths equal on the aperture plane by increasing the electrical length of the ray passing through the center of the lens. For reducing the thickness of a lens with a small F/D, the electrical length of the ray passing through the center of the lens should be increased. To lengthen the ray path through the thin lens, the lens must be constructed with a dielectric material with high relative permittivity. The slow wave propagates in the dielectric material. Hence, the effective electrical path length increases with respect to the physical pass length of the electromagnetic wave. The higher the relative permittivity, the longer the effective electrical length. Therefore, a thin dielectric lens can be constructed using a dielectric material with high relative permittivity.

B. RECTANGULAR PERIODIC MATCHING STRUCTURE

This subsection describes the equivalent circuit representation of the principle of the MS implemented on the lens surface. Furthermore, an approximate geometric representation of the ideal ML is presented. The higher the relative permittivity of the dielectric used in the lens, the thinner the lens that can be realized. However, when the relative permittivity of the lens is much larger than the permittivity of free space, spatial impedance mismatch cannot be ignored. Owing to the characteristic impedance mismatch between free space and the lens, the incident wave into the lens is reflected. Consequently, the gain of the lens antenna deteriorates.

In this study, the reflected wave on a high permittivity lens surface was suppressed by implementing an impedance MS on the lens surface. The equivalent circuit representation of the characteristic impedance of the dielectric lens and the MS implemented on the lens surface are shown in Fig. 2. We define the relative permittivity of the dielectric that composes the lens as ε_r. We consider that a transverse electromagnetic mode (TEM) wave is incident on the lens and the free space in particular. The relationship between the intrinsic impedance Z_0 in free space and the characteristic impedance in the lens $Z_{L.}$ is as follows [23]

$$Z_L = \sqrt{\frac{\mu_0}{\varepsilon_r \varepsilon_0}} = \sqrt{\frac{1}{\varepsilon_r}} Z_0 \tag{1}$$

where ε_0 and μ_0 are the permittivity and permeability of free space, respectively.

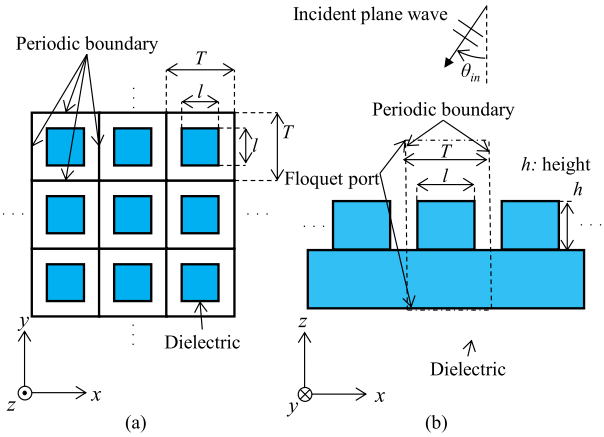

FIGURE 3. Periodic simulation model of the square-pillar periodic structure with plane-wave incidence. (a) Top view and, (b) section.

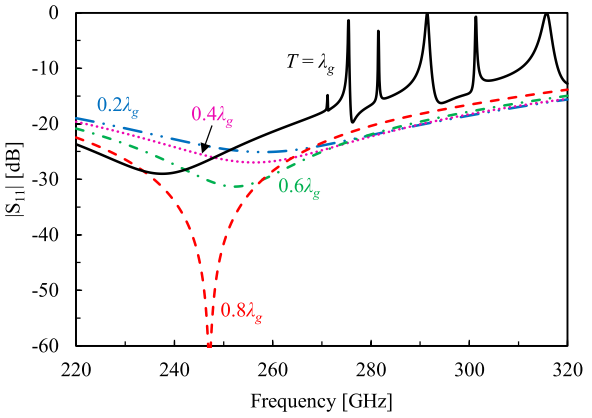

FIGURE 4. Effect on the reflection coefficient S_{11} frequency characteristics when changing the period cycle of the MS, T. Plane waves are incident vertically from the $+z$ direction (TEM wave incident). The space occupancy ratio p was fixed at 0.49.

When the relative permittivity of the lens is $\varepsilon_r \neq 1$, a reflected wave is generated owing to the impedance mismatch between the free space and the lens surface. The reflection coefficient Γ at the boundary is as follows [24].

$$\Gamma = \frac{Z_L - Z_0}{Z_L + Z_0} = \frac{\sqrt{\varepsilon_r} - 1}{\sqrt{\varepsilon_r} + 1}. \tag{2}$$

As shown in (2), when the relative permittivity of the lens is greater than 1, the absolute value of the reflection coefficient is larger. Because the electromagnetic wave reflected on the lens surface does not contribute to the radiation to the front of the antenna, using a material with a large relative permittivity for the lens results in a decrease in the front gain of the lens antenna. To reduce the reflected wave by alleviating impedance mismatch, we consider loading a quarter wavelength, λ_g /4 impedance transformer on the lens surface, as shown on the left side of Fig. 2 (b) [25]. λ_g is the wavelength in the dielectric ML, and it has a relationship $\lambda_g = \lambda_0/\sqrt{\varepsilon_M}$ with a free space wavelength λ_0 and relative permittivity ε_M of the ML. To match the impedance at the boundary between the free space and the ML, the intrinsic in the matching layer impedance Z_M. is derived as follows;

$$Z_M = \sqrt{Z_0 Z_L} = \frac{Z_0}{\sqrt[4]{\varepsilon_r}} \tag{3}$$

To realize (3), the relative permittivity of the ML should be set to $\varepsilon_M = \sqrt{\varepsilon_r}$. However, considering the processability of dielectric materials, manufacturing a dielectric lens with an ML by completely adhering to two types of material with different relative permittivities is challenging. Finding a material with the desired relative permittivity is difficult. Therefore, this study realizes the λ_g /4 ML on the lens surface by machining a square-pillar periodic structure, as shown in the right figure of Fig. 2 (b).

Such a micro dielectric structure has a relative permittivity between that of space and the dielectric material; its effective permittivity is determined based on the space occupancy of the free space and the dielectric. This study realized, an arbitrary effective relative permittivity using a periodic structure, as shown in Fig. 3. The exact shape was periodically formed in two dimensions to facilitate fabrication. The periodic length of the MS is T, the side length of the rectangular cube is l, and the height of the rectangular cube is defined as h. Hence, the space occupancy is defined as follows:

$$p = \left(\frac{l}{T}\right)^2. \tag{4}$$

Focusing on a single period of such a periodic MS, assuming the ratio of the dielectric structure in the periodic plane is p, the effective relative permittivity of the MS ε_{eff} is derived as follows:.

$$\varepsilon_{eff} = \varepsilon_r p + (1 - p), \tag{5}$$

Based on the sub-wavelength structure technique, the impedance matching on the lens surface was achieved by applying a structure with an arbitrary effective permittivity which was obtained by appropriately setting the ratio of the free space and dielectric material.

III. SIMULATION

A. MATCHING STRUCTURE OPTIMIZATION

In this section, the square-pillar periodic MS introduced in Section II is optimized in the 300 GHz band using the electromagnetic (EM) simulator FEKO. To efficiently optimized the matched structure, a single period of the MS was optimized using periodic boundary conditions without the lens and primary radiator, as shown in Fig. 3. The simulation was performed using periodic boundary conditions. The following conditions were assumed. First, the dielectric square-pillar is periodically arranged in the xy-plane. Second, an infinite length of the dielectric exists under a periodic structure. Floquet ports were defined at the upper and lower planes of the periodic simulation model.

A plane wave was incident above the square-pillar with an angle θ_{in}. The permittivity of the bottom and the square-pillar

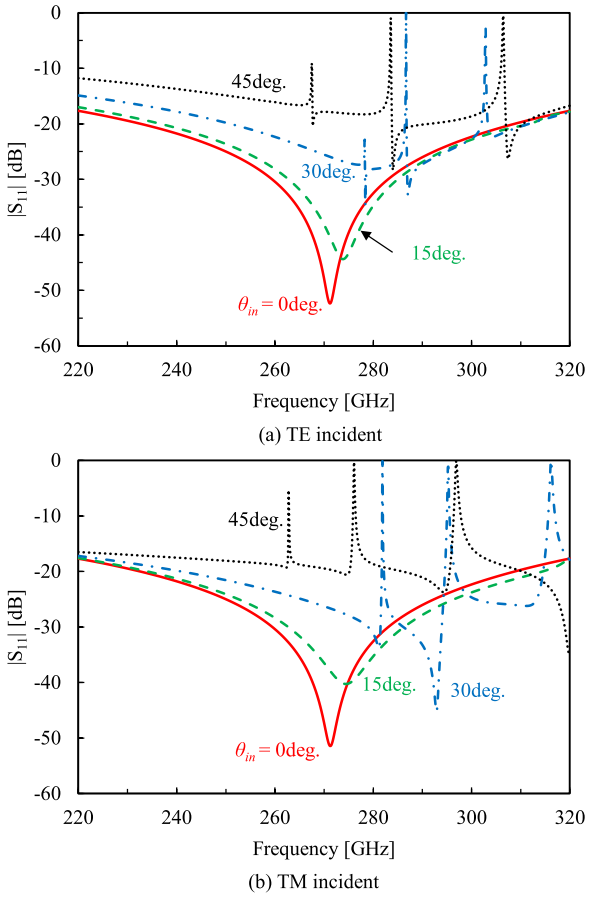

FIGURE 5. Effect on reflection coefficient S_{11} frequency characteristics when changing the plane wave incident angle θ_{in}. (a) represents transverse electric (TE) wave incident, and (b) represents transverse magnetic (TM) wave incident.

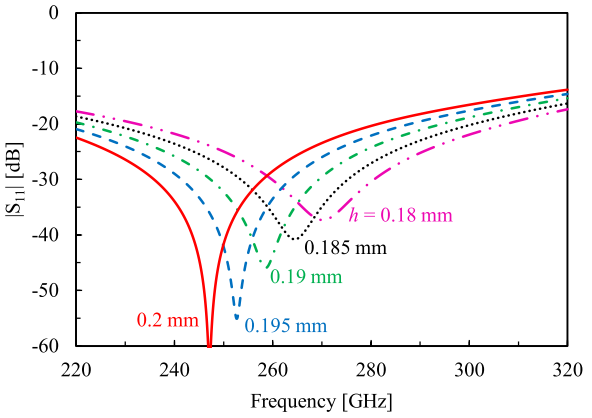

FIGURE 6. Effect of resonance frequency change on reflection coefficient S_{11} caused by the height of the MS, h. The plane wave is incident vertically from the $+z$ direction (TEM wave incident).

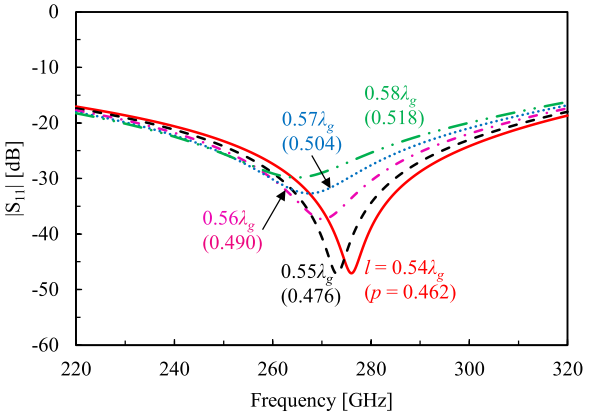

FIGURE 7. Effect on reflection coefficient S_{11} frequency characteristics when changing the rectangular length l. Plane waves are incident vertically from the $+z$ direction (TEM wave incident).

dielectric are equal. This study used, modified-PPE as the the lens material, considering its high relative permittivity, small dielectric loss tangent, and ease of molding, where the relative permittivity ε_r was 5.34 and the dielectric loss tangent was 0.0081. Therefore, the required relative permittivity was $\varepsilon_{eff} \approx 2.31$. The approximate dielectric occupancy that satisfied (3) and (5) was theoretically estimated to be $p \approx 0.4$. The optimum occupancy fluctuated slightly owing to the edge effect of the square-pillar.

As shown in Fig. 3, the MS is optimized based on the reflection coefficient at 270 GHz. The reflection characteristics when the period cycle T is changed are shown in Fig. 4. The occupancy, height, and plane wave incident angle were fixed as $p = 0.49$ (l varies according to T), $h = 0.15$ mm, and $\theta_{in} = 0°$. The side length l change according to T. When T was λ_g, spurious reflections appeared in the S_{11} characteristics, indicating that its operation as an anti-reflection structure was inappropriate. The spurious reflection is caused by a change in the mode propagating inside the MS from the eigenmode [26]. In the case of TEM incidence, to avoid unnecessary spurious results, the period of the MS must satisfy the following equation:

$$T < \frac{\lambda_0}{\sqrt{\varepsilon_{eff}}}. \tag{6}$$

To implement the rectangular MS on the lens, electromagnetic waves were incident perpendicular to the MS at the center of the lens. By contrast, waves are incident obliquely to the MS at the end of the lens. The frequency characteristics of S_{11} when the wave incident angle θ_{in} is varied are shown in Fig. 5. The parameters of the periodic structure are $T = 0.8\lambda_g$, $l = 0.38\lambda_g$ ($p = 0.476$), and $h = 0.183$mm. The larger the incident angle θ_{in}, the higher the resonance frequency of the MS unit cell. A spurious result is generated at $\theta_{in} = 30°$ and 45°. The generation of spurious result can only be avoided by reducing the period T of the MS. Therefore, the period T of the MS must be chosen by considering the angle from the primary radiator to the lens end. In the MS used in this study, the reflected waves were generated at the top and bottom points of the square-pillar periodic MS. When the MS is optimized considering obliquely incident waves, the MS will be

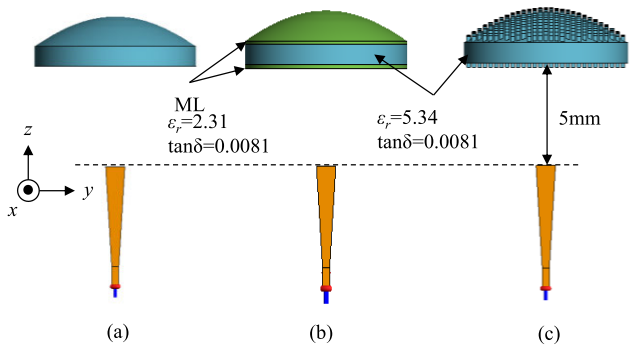

FIGURE 8. Simulation of the lens antenna structure (a) without anti-reflection structure (b) with a planar ML, and (c) with an MS at the top and bottom.

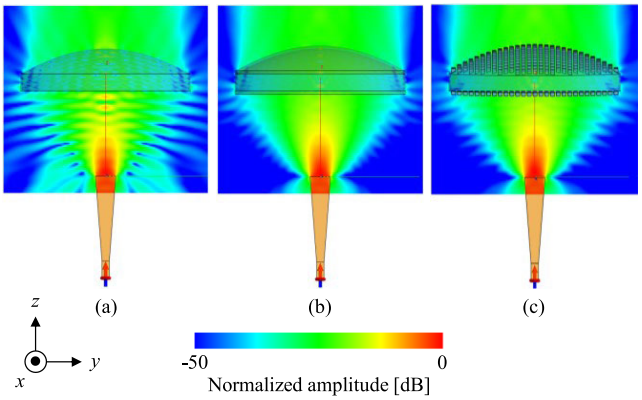

FIGURE 9. Near-field amplitude distributions in a section of the lens antenna. (a) Without anti-reflection structure (b) with an ML at the top and bottom, and (c) with an MS at the top and bottom.

effective even if the MS is added to a curved surface other than a plano-convex lens. The highest performance was exhibited at the frequency at which these two reflected waves canceled out. Ideally, this frequency is $\lambda_g/4$ as described in Section II; however, it is actually influenced by the edges of square-pillar periodic. Thus, the rectangular height h should be optimized for the reflection characteristics at the design frequency. The S_{11}frequency characteristics when the rectangular height h is changed are shown in Fig. 6, where the periodic length and occupancy ratio are fixed as $T = 0.8\lambda_g$, and $l = 0.39\lambda_g$ ($p = 0.49$), respectively. As mentioned earlier, the resonance frequency changed with h; the resonant frequency is lower when the height h is higher. The effective relative permittivity determines the impedance-matching characteristics of a square-pillar periodic MS. The theoretical desired effective permittivity is expressed in (5), and the spatial occupancy that realized the permittivity is expressed in (4); however, p should be optimized by EM simulation as well as other parameters. The S_{11} frequency characteristics with varying l are shown in Fig. 7. The period was fixed at $T = 0.8\lambda_g$. This indicates that the reflection level around the design frequency changes depending on l and p, and the optimum value slightly different from the theoretically appropriate value $p \approx 0.4$. This mainly results from the influence of the edges of the square-pillar periodic structure and dielectric loss tangent. In addition, as p increases, the wavelength in the MS decreases, the resonance frequency shifts slightly to a higher frequency. The reflection characteristics of the rectangular MS can be controlled arbitrarily by adequately designing the aforementioned parameters. First, an efficient optimization is performed to determine the period length T based on the overall structure of the lens, then adjust the resonance frequency according to the rectangular height h, and finally, optimize the rectangular length l. Moreover, it is challenging for fabrication in the 300GHz band if the size of the single period of square-pillar periodic is too large and asymmetrical, therefore, the shape of the single periodic square-pillar periodic structure is designed with symmetrical for ease of fabrication.

B. LENS ANTENNA PERFORMANCE

The antenna efficiency is an index used to evaluate the characteristics of the lens performance. In this section, a comparison of the design structures is investigated based on the gain and radiation patterns to validate the efficiency between the ideal planar ML and the square-pillar periodic MS. The principles of high-gain performance are compared and described. The simulation structure comparison of the dielectric lens without anti-reflection, lens with ML, and lens with a square-pillar periodic MS, are shown in Fig. 8. The design of the primary radiator is shown in Section II, with a lens diameter of D and focal length F of 5 mm. The planar ML structure was designed based on the quarter-wavelength impedance transformer mentioned in Section II-B. The square-pillar periodic MS is a design based on the study of the periodic simulation in Section III-A. The near-field amplitude distribution of the lens antenna without anti-reflection, with ML at the top and bottom surfaces, and the square-pillar periodic MS at the top and bottom surfaces in shown in Fig. 9.

As shown in Fig. 9 (a), the near-field distribution without the anti-reflection structure has strong standing waves both in the lens and between the primary radiator and the lens owing to direct radiation from the primary radiator and the reflected wave on the lens surface. In addition, such a lens surface-reflected wave becomes an unnecessary radiation incident obliquely behind the lens. Furthermore, in the absence of an anti-reflection surface, the radiation in the oblique direction in front of the lens is disturbed, resulting in an enlarged sidelobe level. Thus, we assumed that forming the lens from a high-permittivity material with an effective impedance MS improves the radiation performance of the entire lens antenna by degrading the lens surface reflection, as shown in Figs. 9 (b) and (c). Furthermore, the lens with ML and the lens with square-pillar periodic MS assisted in suppressing the standing waves between the lens and the primary radiator.

The main polarization far-field patterns and gain frequency characteristics in the comparison of the lens without anti-reflection, lens with ML, and lens with MS are shown in

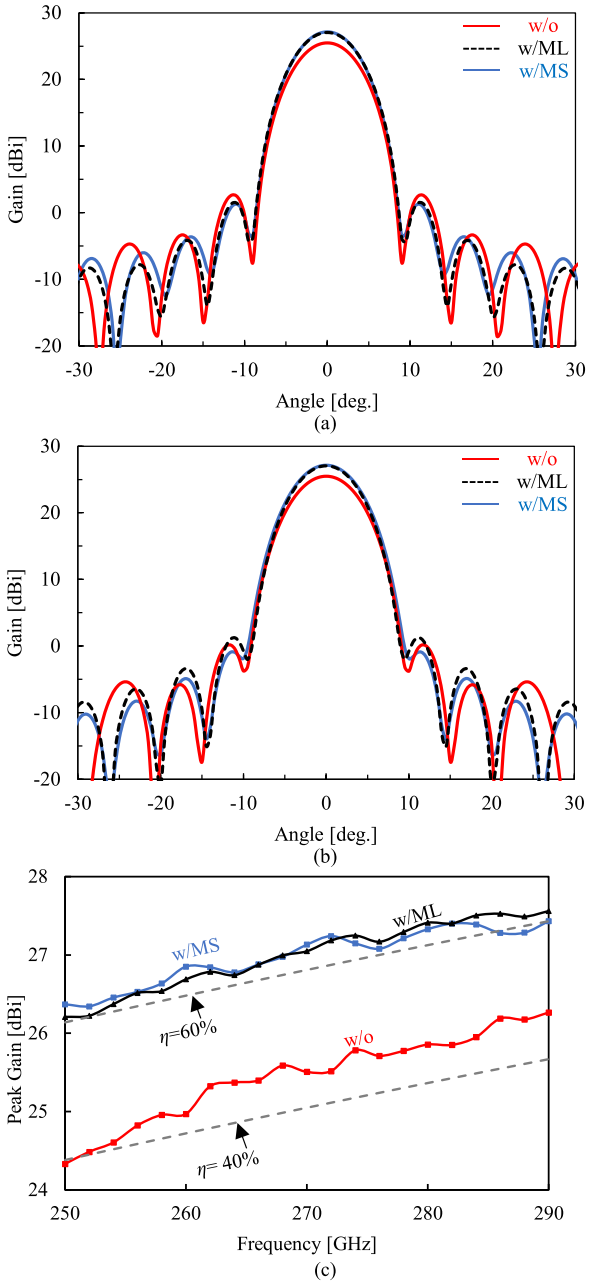

FIGURE 10. Main polarization far-field comparison of the lens without anti-reflection, comprises an ML and anti-reflection square-pillar periodic MS. (a) E-plane radiation pattern at 270GHz, (b) H-plane radiation pattern at 270 GHz and, (c) gain vs. frequency.

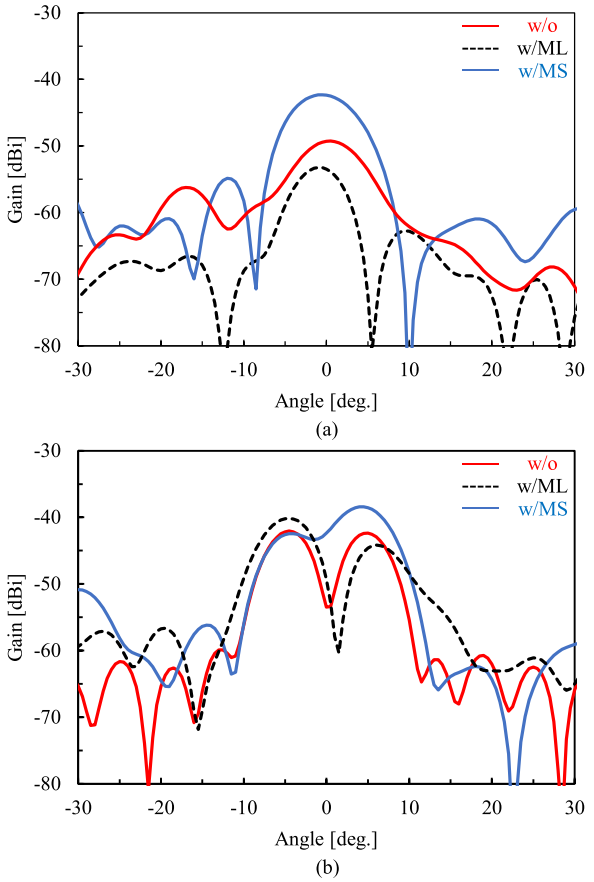

FIGURE 11. Cross-polarization far-field comparison of the lens without anti-reflection, comprising an ML and anti-reflection square-pillar periodic MS. (a) E-plane radiation pattern at 270GHz and, (b) H-plane radiation pattern at 270 GHz.

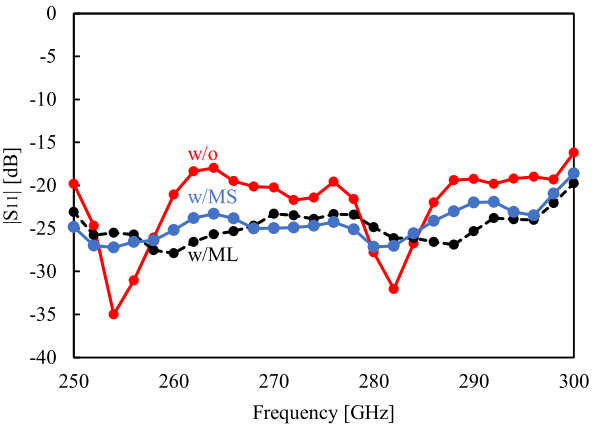

FIGURE 12. Comparison of the reflection coefficient S_{11} of the lens without anti-reflection, comprising an ML and anti-reflection square-pillar periodic MS.

Fig. 10. As shown in Figs. 10 (a), and (b), the lens with ML and MS produced lower sidelobe levels compared with those without anti-reflection structure lens. The lens with MS clearly achieves the anti-reflection function with a single material and the same radiation performance as the lens with planar ML. As shown in Fig. 10 (c), the lens with an MS indicates that the gain increased over a wide bandwidth, not limited to the designed frequency of 270 GHz only. In addition by implementing the lens with the MS, the antenna aperture efficiency increased from 40% to 60% (an improvement of approximately 2dB). Furthermore, as shown in Fig. 11, the lens with MS is not as low as the lens with ML, however, the cross-polarization level was maintained sufficiently low.

Therefore the designed MS is sufficiently compelling from a manufacturing viewpoint, as lenses with an anti-reflection

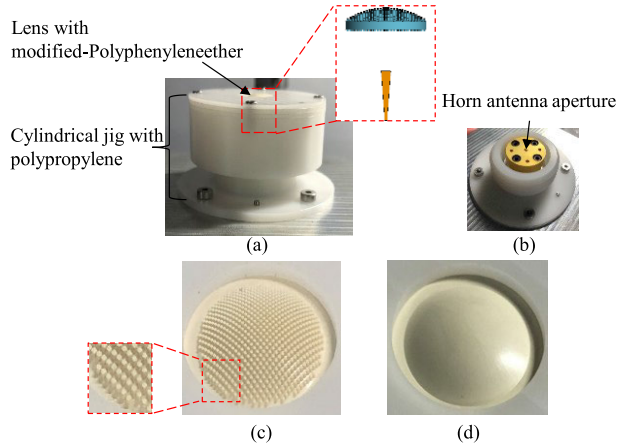

FIGURE 13. Fabricated lenses and primary radiator. (a) overall structure, (b) primary radiator excluding the lens, (c) lens with square-pillar periodic MS, and (d) lens without anti-reflection structure.

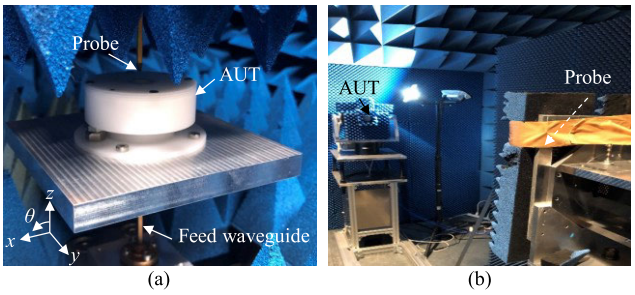

FIGURE 14. Measurement setup of planar (a) near-field, and (b) far-field.

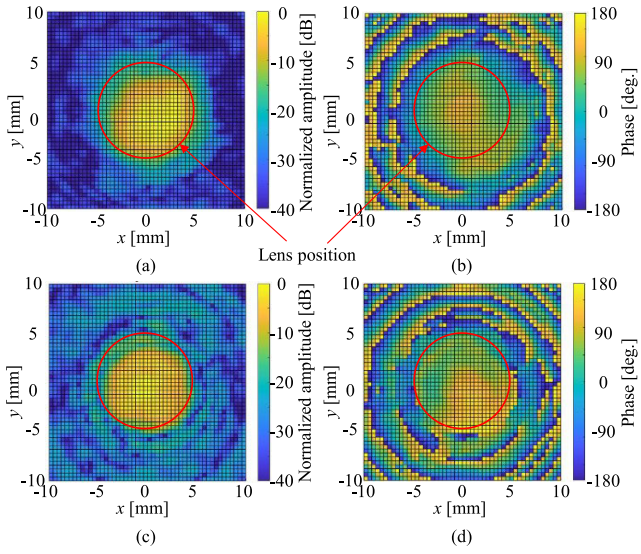

FIGURE 15. Near-field distribution over the parallel plane of the fabricated lens antenna aperture. The left and right column represents the normalized amplitude, and phase angle respectively. (a) and, (b) are with the MS lens, while (c) and, (d) are the without MS lens.

function can be constructed from a single material. The simulation comparison performance for reflection coefficient S_{11} of the lens without anti-reflection, a lens with ML, and a lens with MS is shown in Fig. 12.

All three types of lens reflection coefficients are above −10 dB band range from 250 to 300 GHz; however, the lens with ML and lens with MS can improve the reflection coefficient to higher above than the −20 dB band from 250 to 290 GHz. This proves lens with MS provides a better reflection coefficient.

IV. EXPERIMENTAL SETUP AND RESULTS

We designed a prototype lens with an MS and evaluated its radiation characteristics to validate the simulation. The fabricated proposed lens antennas are shown in Fig. 13. The overall structure is shown in Fig. 13 (a) and the primary radiator, excluding the lens is shown in Fig. 13 (b). The primary radiator had a total height of 5 mm horn antenna, with the primary radiation pattern at the lens edge level −10 dB. A cylindrical jig fixed the lens shown in Fig. 13 (c) or (d) at a position 10 mm from the aperture of the horn. The designed lenses had a curved surface with a diameter length of 10 mm. A square-pillar periodic MS on the lens surface is shown in Fig. 13 (c). As shown in the cylindrical jig made of polypropylene, these lenses are composed of a modified-PPE with $\varepsilon_r = 5.34$, and $\tan\delta = 0.0081$. A cylindrical jig with Polypropylene material with $\varepsilon_r = 2.4$ and $\tan\delta = 0.001$ was used to hold the lens and horn together. The end thickness of the dielectric lens was fixed at 1 mm to the jig.

The horn antenna was connected to a WR-3 standard waveguide for the feeding. The measurement setup is shown in Fig. 14. The radiation pattern of the lens antenna in this study was obtained using planar near-field measurements, as shown in Fig. 14 (a) [27]. The near-field is acquired from a distance of 2 mm from the lens top, in an area of 20-dB dynamic range concerning the peak magnitude to avoid leakage of radiant energy acquisition. In addition, the sampling pitch was set to 0.5 mm to evaluate the radiation characteristics up to frequency of 290 GHz. Far-field measurements, to determine the absolute gain of the fabricated antenna compared with the standard gain horn antenna as shown in Fig. 14 (b). The distance between the antenna under test (AUT) and the far-field probe was set to 2 m to satisfy the far-field conditions, including the cylindrical jig.

The measured near-field distributions are shown in Fig. 15. The lens diffraction in amplitude and phase distribution without an anti-reflection surface structure can be seen as higher and less diffraction, respectively. In particular, without the anti-reflection structure, the amplitude was significantly disturbed outside the aperture of the lens. The disturbance caused the deterioration of the radiation performance. The radiation patterns at 270 GHz and the frequency response of the lens gain with and without the anti- reflection structures are shown in Fig. 16. The gain was measured by comparison method with a standard gain horn whose gain was measured by extrapolation technique. The measurement results are shown as solid lines, whereas the simulation results as shown as dashed and broken lines. E-plane radiation pattern

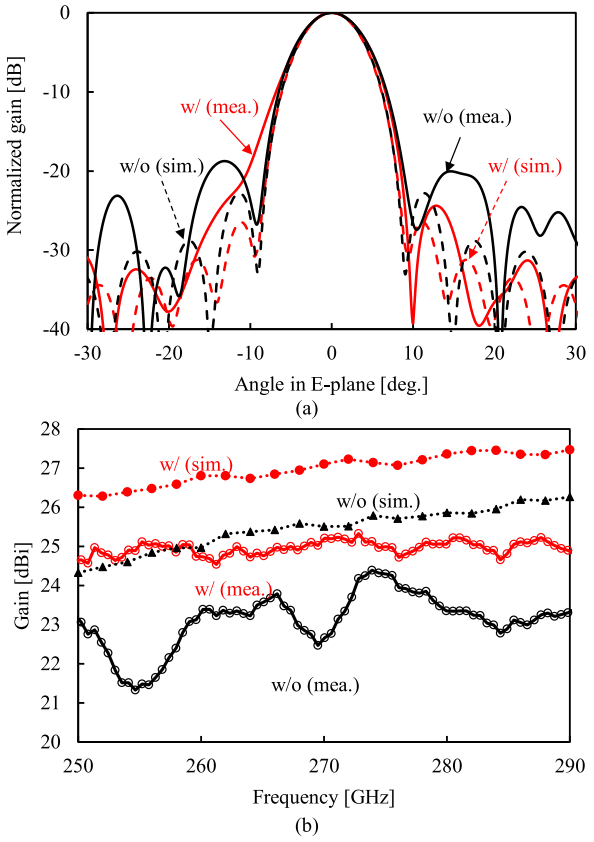

FIGURE 16. Comparison of lens antennas with and without a square-pillar periodic anti-reflection structure. (a) Radiation pattern and, (b) gain patterns vs. frequency.

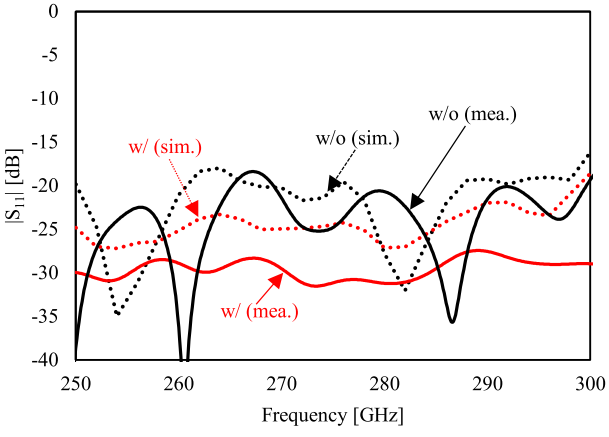

FIGURE 17. Comparison of the reflection coefficient S_{11} of the lens without anti-reflection, and lens with square-pillar periodic MS.

at 270 GHz is shown in Fig. 16 (a). The main beam became sharper, and the sidelobe level decreased by forming a rectangular periodic MS, unlike the case without an anti-reflection structure. As shown in Fig. 16 (b), the frequency response of the measured gain was lower than that of the simulation results, depending on the frequency. However overall, the measured lens with the anti-reflection structure showed high gain increases in all bands compared with the lens without anti-reflection. The gain increase between the two lens types was approximately 2 dB, except at 275 GHz. The discrepancy between the simulation and measurement results can be attributed to dielectric losses in the lens and conductor losses in the primary radiator. The simulated and measured reflection coefficients S_{11} of the lens antennas with and without MS are shown in Fig. 17. The radiated wave from the horn is reflected at the lens center back and received again, which increases reflection coefficient S_{11}. However, S_{11} of the lens antenna is reduced by using MS. The reflection level fluctuates due to the interference between the reflections from the horn antenna and the lens surface. The maximum reflection level was approximately −20 dB. On the other hand, with MS, the reflection characteristic should be almost identical to that of the individual horn antenna. The simulated and measured reflection levels were approximately −25 dB and −30 dB, respectively. Based on the aforementioned measurement results, the amount of radiation performance improvement perfectly agreed with the simulation results. Although the performance of the measured results performance is slightly degraded compared to simulation results, the proposed antenna architecture is well validated. The effectiveness of the implemented impedance ML was demonstrated.

V. CONCLUSION

A dielectric lens antenna with an anti-reflection structure based on the spatial impedance matching theorem in 300 GHz band was developed. The square-pillar periodic MS implemented on the lens surface was made of the same dielectric material as the lens, considering fabrication feasibility. The periodic MS was optimized using a unit cell electromagnetic simulation, and the derived optimal MS was added to the surface of the dielectric lens. Through simulations and experiments, we validated that the square-pillar periodic MS reduced the reflection wave on the lens surface, and the peak gain of the lens antenna was improved by about 2 dB between 250 GHz to 290 GHz. Low-cost and high-efficiency lens antennas are expected for the applications of future high-bitrate and mobile communication systems.

REFERENCES

[1] M. Tamosiunaite, S. Tamosiunas, M. Zilinskas, and G. Valusis, "Atmospheric attenuation of the terahertz wireless networks," in *Broadband Communications Networks—Recent Advances and Lessons From Practice*. U.K.: IntechOpen, Sep. 2018.

[2] G. Ducournau, P. Szriftgiser, F. Pavanello, E. Peytavit, M. Zaknoune, D. Bacquet, A. Beck, T. Akalin, and J. Lampin, "THz communications using photonics and electronic devices: The race to data-rate," *J. Infr., Millim., Terahertz Waves*, vol. 36, no. 2, pp. 198–220, Feb. 2015.

[3] T. Kleine-Ostmann and T. Nagatsuma, "A review on terahertz communications research," *J. Infr., Millim. Terahertz Waves*, vol. 32, no. 2, pp. 143–171, 2011.

[4] P. Baron, J. Mendrok, Y. Kasai, S. Ochiai, T. Seta, K. Sagi, K. Suzuki, H. Sagawa, and J. Urban, "AMATERASU: Model for atmospheric terahertz radiation analysis and simulation," *J. Nat. Inst. Inf. Commun. Technol.*, vol. 55, no. 1, pp. 109–121, Jan. 2018.

[5] W. Jiang, B. Han, M. A. Habibi, and H. D. Schotten, "The road towards 6G: A comprehensive survey," *IEEE Open J. Commun. Soc.*, vol. 2, pp. 334–366, 2021.
[6] Y. He, Y. Chen, L. Zhang, S.-W. Wong, and Z. N. Chen, "An overview of terahertz antennas," *China Commun.*, vol. 17, no. 7, pp. 124–165, Jul. 2020.
[7] Y. J. Guo, M. Ansari, R. Ziolkowski, and N. J. G. Fonseca, "Quasi-optical multi-beam antenna technologies for B5G and 6G mmWave and THz networks: A review," *IEEE Open J. Antennas Propag.*, vol. 2, pp. 807–830, 2021.
[8] R. Ishihara, K. Sakakibara, N. Kikuma, Y. Sugimoto, Y. Yamada, and N. H. Abd Rahman, "Measured performance of high gain dielectric lens antenna in 300 GHz band," in *Proc. Int. Symp. Antennas Propag. (ISAP)*, Osaka, Japan, Jan. 2021, pp. 17–18.
[9] P. Kadera, T. Mikulasek, J. Hruska, and J. Lacik, "Hyperbolic lens horn antenna for fixed-beam E-band communication," in *Proc. 30th Int. Conf. Radioelektronika (RADIOELEKTRONIKA)*, Apr. 2020, pp. 1–5.
[10] Y. Tajima and Y. Yamada, "Simulations of a shaped dielectric lens antenna by FEKO," *Appl. Comput. Electromagn. Soc. J.*, vol. 24, no. 4, pp. 419–426, Jun. 2009.
[11] R. A. dos Santos, G. Lobão da Silva Fré, L. G. da Silva, M. C. D. Paiva, and D. H. Spadoti, "Ultra-wideband dielectric lens antennas for beamsteering systems," *Int. J. Antennas Propag.*, vol. 2019, pp. 1–8, Aug. 2019.
[12] B. Baharom, Y. Sugimoto, K. Sakakibara, B. Rohani, N. Kikuma, and Y. Yamada, "Design for uniform aperture distribution of 2×2 lens array using concave-convex lens in THz band," in *Proc. Int. Symp. Antennas Propag. (ISAP)*, Sydney, NSW, Australia, Oct./Nov. 2022, pp. 123–124.
[13] S. Van Berkel, M. Alonso-Delpino, C. Jung-Kubiak, and G. Chattopadhyay, "Low-profile and high-gain submm-wave lens antenna for compact instruments," in *Proc. 16th Eur. Conf. Antennas Propag. (EuCAP)*, Madrid, Spain, Mar. 2022.
[14] H. Yi, S.-W. Qu, K. B. Ng, and C. H. Chan, "3-D printed discrete dielectric lens antenna with matching layer," in *Proc. Int. Symp. Antennas Propag. Conf.*, Taiwan, Dec. 2014, pp. 115–116.
[15] P. Lalanne and G. M. Morris, "Antireflection behavior of silicon subwavelength periodic structures for visible light," *Nanotechnology*, vol. 8, no. 2, pp. 53–56, Jun. 1997.
[16] S. J. Wilson and M. C. Hutley, "The optical properties of 'moth eye' antireflection surfaces," *Optica Acta: Int. J. Opt.*, vol. 29, no. 7, pp. 993–1009, Dec. 2010.
[17] Mitsubishi Chem. Corporation. *M-Polyphenylene Ether Resin (M-PPE Resin) 'LEMALLOY': Products*. Accessed: 2022. [Online]. Available: https://www.m-chemical.co.jp/en/products/departments/group/mep/product/1201413_7826.html
[18] E. Peters, "Poly(phenylene ether) based amphiphilic block copolymers," *Polymers*, vol. 9, no. 12, p. 433, Sep. 2017.
[19] P. F. Goldsmith, *Quasioptical Systems: Gaussian Beam Quasioptical Propogation and Applications*. Hoboken, NJ, USA: Wiley, 1998, pp. 1–430.
[20] R. C. Johnson, *Antenna Engineering Handbook*, 3rd ed. New York, NY, USA: McGraw-Hill, 1993, sec. 16-2, p. 16-6.
[21] R. Brown, "Dielectric bifocal lenses," in *Proc. IRE Int. Conv. Rec.*, New York, NY, USA, 1966, pp. 180–187.
[22] A. L. Peebles, "A dielectric bifocal lens for multibeam antenna applications," *IEEE Trans. Antennas Propag.*, vol. AP-36, no. 5, pp. 599–606, May 1988.
[23] W. L. Stutzman and Gary A. Thiele, *Antenna Theory and Design*. Hoboken, NJ, USA: Wiley, Sec. 1.11, 1981, pp. 64–65.
[24] W. L. Curtis, "Effect of lossy Earth on antenna gain, Part 2," *J. Res. Nat. Bur. Standards, D, Radio Sci.*, vol. 68D, no. 7, p. 813, Jul. 1964.
[25] W. Harris, T. Nichols, M. Abbasi, and D. Ricketts, "A versatile mm-wave micromachined anti-reflective layer," in *Proc. Asia–Pacific Microw. Conf. (APMC)*, New Delhi, India, Dec. 2016, pp. 4–7.
[26] H. Kikuta, H. Toyota, W. Yu, A. Mizutani, and K. Iwata, "Optical elements with subwavelength structured surfaces," *Proc. SPIE*, vol. 5515, p. 125, Oct. 2004.
[27] A. D. Yaghjian, "An overview of near-field antenna measurements," *IEEE Trans. Antennas Propag.*, vol. AP-34, no. 1, pp. 30–45, Jan. 1986.

BAZILAH BAHAROM (Student Member, IEEE) was born in Penang, Malaysia, in 1994. She received the Bachelor of Engineering degree (Hons.) in electronic engineering from Universiti Teknologi MARA, Malaysia, in 2018, and the Master of Science degree in electrical engineering from the Antenna Research Centre (ARC), Faculty of Electrical Engineering, Universiti Teknologi MARA, in 2020. She is currently pursuing the Ph.D. degree with the Department of Electrical and Mechanical Engineering, Nagoya Institute of Technology, Nagoya, Japan. Her current research interests include dielectric lens antenna and lens array antennas for millimeter-wave applications.

RYOTA ISHIHARA was born in Aichi, Japan. He received the B.Sc. and M.Sc. degrees from the Nagoya Institute of Technology, Aichi, in 2020 and 2022, respectively. His research interest includes dielectric lens antenna.

YOSHIKI SUGIMOTO (Member, IEEE) was born in Fukui, Japan. He received the B.Sc. and M.Sc. degrees from the University of Fukui, Fukui, in 2013 and 2015, respectively, and the Ph.D. degree from Yokohama National University, Yokohama, Japan, in 2018. From 2018 to 2020, he was at Omron Corporation, where he was involved in the development of wireless power transfer systems and millimeter radar signal processing. In 2020, he joined the Nagoya Institute of Technology as an Assistant Professor. His research interests include antenna measurement and scattering problems.

KUNIO SAKAKIBARA (Senior Member, IEEE) was born in Aichi, Japan, in 1968. He received the B.S. degree in electrical and computer engineering from the Nagoya Institute of Technology, Nagoya, Japan, in 1991, and the M.S. and D.E. degrees in electrical and electronic engineering from the Tokyo Institute of Technology, Tokyo, Japan, in 1993 and 1996, respectively. From 1996 to 2002, he was at the Toyota Central Research and Development Laboratories Inc., Nagakute, where he was involved in the development of antennas for automotive millimeter-wave radar systems. From 2000 to 2001, he was a Guest Researcher at the Department of Microwave Techniques, University of Ulm, Ulm, Germany. In 2002, he joined the Nagoya Institute of Technology as a Lecturer. Since 2004, he has been an Associate Professor, and became a Professor with the Nagoya Institute of Technology, in 2012. His current research interests include millimeter-wave antennas and feeding circuits.

NOBUYOSHI KIKUMA (Senior Member, IEEE) was born in Ishikawa, Japan, in 1960. He received the B.S. degree in electronic engineering from the Nagoya Institute of Technology, Japan, in 1982, and the M.S. and Ph.D. degrees in electrical engineering from Kyoto University, Japan, in 1984 and 1987, respectively. From 1987 to 1988, he was a Research Associate at Kyoto University. In 1988, he joined the Nagoya Institute of Technology, where he has been a Professor, since 2001. His current research interests include adaptive and signal processing arrays and multipath propagation analysis, mobile and indoor wireless communication, and electromagnetic field theory. He was a recipient of the 4th Telecommunications Advancement Foundation Award, in 1989.

TAKAYUKI ARAI was born in Tokyo, Japan. He joined Enplas Corporation, in 1991. He engaged in development of several plastic lenses. Since 2020, he was responsible for development lens prototype manufacturing.

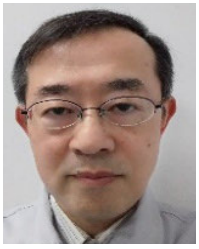

TAKAYOSHI SUGANUMA was born in Aichi, Japan, in 1965. He joined Enplas Corporation, in 2002. He engaged in development of optical components.

TOMOHIRO SAITO was born in Saitama, Japan. He joined Enplas Corporation, in 1994. He engaged in optical design in the visible light range.